Cancer Cell
Article

Therapeutic Effect of γ-Secretase Inhibition in *Kras*^{G12V}-Driven Non-Small Cell Lung Carcinoma by Derepression of DUSP1 and Inhibition of ERK

Antonio Maraver,[1,*] Pablo J. Fernandez-Marcos,[1,12] Daniel Herranz,[1,9,12] Marta Cañamero,[2] Maribel Muñoz-Martin,[1] Gonzalo Gómez-López,[3] Francisca Mulero,[4] Diego Megías,[5] Marta Sanchez-Carbayo,[6] Jie Shen,[7] Montserrat Sanchez-Cespedes,[8] Teresa Palomero,[9,10] Adolfo Ferrando,[9,10,11] and Manuel Serrano[1,*]
[1]Tumor Suppression Group
[2]Comparative Pathology Unit
[3]Bioinformatics Unit
[4]Molecular Imaging Unit
[5]Confocal Microscopy Unit
[6]Tumor Markers Group
Spanish National Cancer Research Centre, E-28029 Madrid, Spain
[7]Center for Neurologic Diseases, Brigham and Women's Hospital and Harvard Medical School, Boston, MA 02115, USA
[8]Cancer Epigenetics and Biology Program, Bellvitge Biomedical Research Institute, 08007 Barcelona, Spain
[9]Institute for Cancer Genetics
[10]Department of Pathology
[11]Department of Pediatrics
Columbia University Medical Center, New York, NY 10032, USA
[12]These authors contributed equally to this work
*Correspondence: amaraver@cnio.es (A.M.), mserrano@cnio.es (M.S.)
http://dx.doi.org/10.1016/j.ccr.2012.06.014

SUMMARY

Here, we have investigated the role of the Notch pathway in the generation and maintenance of *Kras*^{G12V}-driven non-small cell lung carcinomas (NSCLCs). We demonstrate by genetic means that γ-secretase and RBPJ are essential for the formation of NSCLCs. Of importance, pharmacologic treatment of mice carrying autochthonous NSCLCs with a γ-secretase inhibitor (GSI) blocks cancer growth. Treated carcinomas present reduced HES1 levels and reduced phosphorylated ERK without changes in phosphorylated MEK. Mechanistically, we show that HES1 directly binds to and represses the promoter of *DUSP1*, encoding a dual phosphatase that is active against phospho-ERK. Accordingly, GSI treatment upregulates DUSP1 and decreases phospho-ERK. These data provide proof of the in vivo therapeutic potential of GSIs in primary NSCLCs.

INTRODUCTION

Lung cancer is the leading cause of cancer-related deaths in the world. A major challenge in treating lung cancer is to find novel therapeutic targets that can complement current chemotherapy.

The Notch pathway is highly complex and regulates various processes, such as embryonic development, cell fate decisions, and tissue homeostasis, and it has been implicated in a variety of human diseases, including cancer (Chiba, 2006; Demarest et al., 2008; Ferrando, 2009; Hass et al., 2009; Roy et al., 2007). Briefly, this pathway involves a total of five activatory ligands, four NOTCH receptors, sequential proteolytic processing of the ligand-bound receptors to generate active Notch intracellular domains (NICDs), and formation of DNA-binding complexes

Significance

NOTCH1 oncogenic mutations have been found in T cell leukemias and lung cancer. In T cell leukemias, the Notch pathway activates AKT and NFκB through HES1-mediated transcriptional repression of *PTEN* and *CYLD*, respectively. Little is known, however, about how the Notch pathway participates in lung cancer. Here, we show that Notch pathway inhibition, either genetically or pharmacologically, hampers primary *Kras*^{G12V}-driven non-small cell lung carcinomas (NSCLCs). We demonstrate that HES1 directly represses the promoter of *DUSP1*, which encodes a dual-specificity phosphatase with activity against phospho-ERK. Treatment with GSIs induces *DUSP1* expression, and this is associated with loss of ERK phosphorylation, a critical player in NSCLCs. These results validate the potential of GSIs for the treatment of primary NSCLCs.

with a number of DNA-binding partners, with RBPJ being the most important and the one that defines the so-called "canonical" Notch pathway (Chiba, 2006; Demarest et al., 2008; Ferrando, 2009; Heitzler, 2010; Roy et al., 2007). In turn, NICD-containing complexes activate the expression of a number of effectors, including the transcriptional repressor HES1 (Sang et al., 2010).

The γ-secretase complex is essential for the Notch pathway because it is responsible for the activation of NOTCH receptors by proteolytic cleavage (Hass et al., 2009). This complex is formed by the assembly of four protein subunits, namely, a presenilin subunit (PSEN1 or PSEN2), nicastrin (NCSTN), APH1, and PSNEN (Fraering, 2007). The proteolytic activity of the γ-secretase complex occurs within the PSEN subunit; however, each of the four subunits is essential for the formation of a functional γ-secretase complex (Fraering, 2007). In this regard, we have demonstrated that the combined deletion of the PSEN genes *Psen1* and *Psen2* results in ablation of NOTCH1 activation in T cells (Maraver et al., 2007). Additionally, small-molecule inhibitors that target the γ-secretase complex (known as γ-secretase inhibitors [GSIs]) (Wolfe, 2009) phenocopy Notch pathway inhibition in mouse models (van Es et al., 2005; Wong et al., 2004).

The oncogenic role of the Notch pathway is well established in T cell acute lymphoblastic leukemias (T-ALL), and *NOTCH1* is oncogenically mutated in ~60% of leukemias (Ferrando, 2009). Investigators have reported a number of alterations in the Notch pathway in human non-small cell lung carcinomas (NSCLCs), including NOTCH3 overexpression (Haruki et al., 2005); loss of expression of NUMB (Westhoff et al., 2009), a negative regulator of the Notch pathway; and activating mutations in *NOTCH1* (Westhoff et al., 2009). Previous reports have demonstrated that GSIs induce apoptosis in human lung cancer cells grown in vitro (Chen et al., 2007; Eliasz et al., 2010; Westhoff et al., 2009) and slow the growth of subcutaneous xenografts formed by human lung cancer cells (Konishi et al., 2007; Luistro et al., 2009; Paris et al., 2005). However, little is known about the activity of GSIs in primary autochthonous NSCLCs in their natural environment, or about the mechanisms by which GSIs could exert their antitumoral effect on NSCLCs.

In mice, inducible genetic activation of a latent *Kras* oncogenic allele in the lung initiates a stepwise tumorigenic process that culminates in NSCLCs very similar to those found in humans, sharing a common histology (Guerra et al., 2003; Jackson et al., 2001) and a common transcriptional profile (Sweet-Cordero et al., 2005). Therefore, we used this mouse model to analyze the effect of the Notch pathway on the development of NSCLCs.

RESULTS

The Notch Pathway Is Hyperactive in Murine *Kras*^{G12V}-Driven NSCLC

The Notch pathway is hyperactive in a subset of human NSCLCs (Westhoff et al., 2009). Therefore, we wanted to know whether this is also the case for murine *Kras*^{G12V}-driven adenocarcinoma, which is a common type of NSCLC (Guerra et al., 2003). All of the analyzed murine NSCLCs presented significantly higher levels of NICD and HES1 compared with normal lung (Figure 1A). To evaluate the levels of γ-secretase, we measured the abundance of

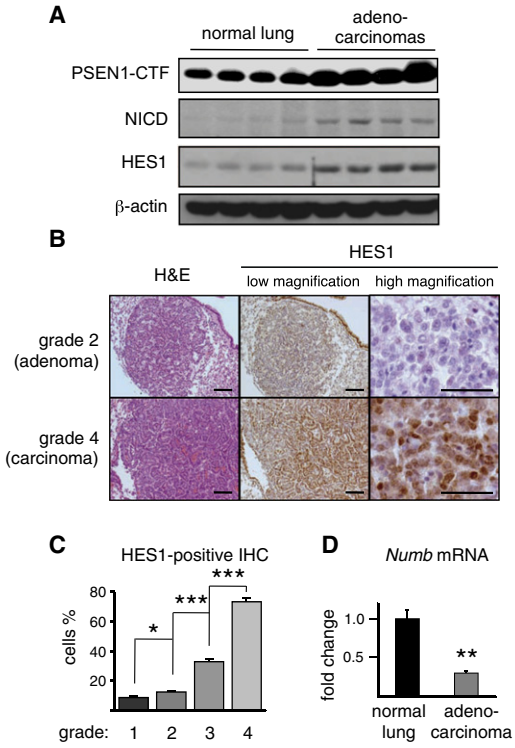

Figure 1. Activity of the Notch Pathway in Murine *Kras*^{G12V}-Driven NSCLC

(A) Analysis of γ-secretase activity by detection of PSEN1-CTF, and analysis of NOTCH1 activity by detection of NICD and HES1 by immunoblotting (normal lung: each lane corresponds to a different control WT mouse; adenocarcinomas: each lane corresponds to a grade 4 tumor from a different mouse).

(B) Detection of HES1 in murine *Kras*^{G12V} lung tumors. Representative examples of grade 2 (adenoma) and grade 4 (adenocarcinoma) tumors stained with hematoxylin and eosin (H&E, left) and HES1 (middle and right) at low magnification (middle) or high magnification (right). Bars in the four leftmost panels correspond to 100 μm. Bars in the two rightmost panels correspond to 50 μm.

(C) Quantification of HES1 during lung tumorigenesis. The graph depicts the percentage of HES1-positive nuclei (detected by IHC as in B) within tumors of different grades (n = 5 for each tumor grade).

(D) Levels of *Numb* mRNA measured by qRT-PCR in WT mouse lungs (n = 4) and grade 4 tumors (n = 4).

Values correspond to the average ± SEM. Statistical significance was determined by a two-tailed Student's t test: *p < 0.05; **p < 0.01; ***p < 0.001.

See also Figure S1.

the active forms of PSEN1 and NCSTN. In the case of PSEN1, assembly into the γ-secretase complex is associated with proteolytic cleavage (Fraering, 2007). We observed higher levels of the carboxy-terminal fragment of PSEN1 (PSEN1-CTF) in murine NSCLCs compared with normal lung (Figure 1A), whereas the levels of *Psen1* mRNA were unchanged (Figure S1A available online). These results agree with a previous study using human fibroblasts cultured in vitro, in which ectopic overexpression of oncogenic *HRAS* was found to increase PSEN1 protein levels without affecting its mRNA levels (Weijzen et al., 2002). In the case of NCSTN, its assembly into the γ-secretase complex is associated with glycosylation and slower electrophoretic mobility (Edbauer et al., 2002). As in the case of PSEN1, we also observed higher levels of mature NCSTN in murine NSCLCs

(Figure S1B). These observations indicate higher levels of functional γ-secretase complex in murine *Kras*^{G12V}-driven NSCLCs.

To define the kinetics of Notch pathway activation during lung tumorigenesis, we tested the expression of HES1 by immunohistochemistry (IHC) in murine lesions at different stages, from grade 1 to grade 4 (with grades 1–3 corresponding to adenomas, and grade 4 to adenocarcinomas) (Jackson et al., 2005). We observed a direct association between tumor grade and HES1 nuclear signal, which reached its maximum in grade 4 lesions (adenocarcinomas; Figures 1B and 1C, and Figure S1C). As an internal control, we also observed strong nuclear expression of HES1 in murine bronchioles (Collins et al., 2004; Ito et al., 2000; Morimoto et al., 2010; Tsao et al., 2009) (Figure S1C). Finally, we found lower levels of expression of *Numb* mRNA (Figure 1D), a negative regulator of the Notch pathway whose expression is also diminished in human NSCLCs (Westhoff et al., 2009). Together, these data indicate that murine *Kras*^{G12V}-driven NSCLCs faithfully recapitulate the activation of the Notch pathway reported in human NSCLCs, validating that this mouse lung cancer model is appropriate for analyzing therapeutic strategies and mechanisms related to the Notch pathway.

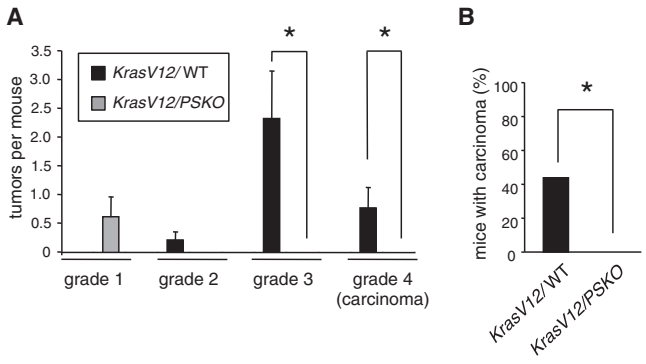

Figure 2. PSEN1 and PSEN2 Are Needed for the Generation of *Kras*^{G12V}-Driven NSCLC

(A) Graph depicting the number and grade of tumors per animal. Lungs from *KrasV12*/WT and *KrasV12/PSKO* mice were pathologically analyzed 5.5–7.5 months after adeno-Cre delivery. For each genotype, n = 9 mice.

(B) Percentage of mice carrying grade 4 (adenocarcinoma) tumors. For each genotype, n = 9 mice.

Values correspond to the average ± SEM. Statistical significance was determined by a two-tailed Student's t test (A) or by Fisher's exact test (B): *p < 0.05.

The γ-Secretase Complex Is Needed for *Kras*^{G12V}-Driven NSCLCs

To evaluate the relevance of the Notch pathway in lung tumorigenesis, we combined a Cre-inducible *Kras*^{G12V} oncogenic allele (*Kras*^{LSLG12Vgeo}) (Guerra et al., 2003) and *Psen1*$^{f/f}$;*Psen2*$^{-/-}$ alleles (i.e., *Psen1* flanked by *loxP* sites excisable by Cre recombinase, and *Psen2* null) (Saura et al., 2004), thus generating compound *Kras*$^{+/LSLG12Vgeo}$;*Psen1*$^{f/f}$;*Psen2*$^{-/-}$ animals. Mice were treated with intratracheal delivery of adeno-Cre (for brevity, we refer to the resulting lungs as *KrasV12/PSKO*). Control mice (*Kras*$^{+/LSLG12Vgeo}$;*Psen1*$^{+/+}$;*Psen2*$^{+/+}$) were derived from the same set of crosses as the *Kras*$^{+/LSLG12Vgeo}$;*Psen1*$^{f/f}$;*Psen2*$^{-/-}$ mice [for brevity, we refer to the adeno-Cre treated lungs as *KrasV12*/wild-type (WT) lungs]. Mice were killed between 5.5 and 7.5 months post-adeno-Cre delivery, and lung tumors were graded and quantified (Figure 2A). Most tumors in control *KrasV12*/WT lungs had progressed to grades 3 and 4; however, in the case of *KrasV12/PSKO* lungs, there was no progression beyond grade 1 (Figure 2A). We also measured the percentage of animals with at least one grade 4 tumor (i.e., adenocarcinoma). Of importance, whereas 44% of *KrasV12*/WT lungs presented adenocarcinomas, none of the *KrasV12/PSKO* lungs developed NSCLCs (Figure 2B).

The Canonical Notch Pathway Is Needed for *Kras*^{G12V}-Driven NSCLCs

Having established the requirement of the γ-secretase complex for generating *Kras*^{G12V}-driven NSCLCs, we wanted to test directly the role of the canonical Notch pathway in this process. To that end, we generated compound mice carrying the Cre-inducible *Kras*^{G12V} oncogenic allele in combination with a floxed allele of *Rbpj*, *Rbpj*$^{f/f}$ (Tanigaki et al., 2002). These mice and their corresponding controls (for brevity, termed *KrasV12/RbpjKO* and *KrasV12*/WT, respectively) were treated by intratracheal delivery of adeno-Cre. It should be noted that in this experiment, the batch of adeno-Cre was more active than in the previous experiment (see Experimental Procedures), and thus yielded a higher number of tumors per mouse. As was the case for the *KrasV12/PSKO* mice, in the *KrasV12/RbpjKO* mice, grade 4 tumors (adenocarcinomas) were absent 5.5–7.5 months post-adeno-Cre delivery (Figures 3A and 3B). We wondered whether the grade 3 tumors present in *KrasV12/RbpjKO* mice had actually deleted the *Rbpj* gene or, alternatively, were nondeleted *Rbpj*-floxed tumors ("escapers"). To address this issue, we microdissected grade 3 tumors (n = 3), and we observed that all of them were escapers (Figure S2). Taken together, the results of our genetic analyses indicate that the Notch pathway is essential for NSCLC formation driven by *Kras*^{G12V}.

Pharmacological Inhibition of γ-Secretase Arrests *Kras*^{G12V}-Driven NSCLCs

Having demonstrated that γ-secretase is highly relevant for lung tumorigenesis, and that the Notch pathway is strongly active in lung cancer, we conducted a preclinical assay to test the impact of γ-secretase inhibition on primary NSCLCs. Previous reports demonstrated that small-molecule inhibitors of the γ-secretase pathway (generally known as GSIs) induce apoptosis in lung cancer cells grown in vitro (Chen et al., 2007; Eliasz et al., 2010; Westhoff et al., 2009) and slow the growth of subcutaneous xenografts formed by lung cancer cells (Konishi et al., 2007; Luistro et al., 2009; Paris et al., 2005). However, nothing is known about the impact of GSIs on autochthonous primary NSCLCs, i.e., in their natural microenvironment. For this assay, we used compound LSN-411575 (Wong et al., 2004). This compound has been well validated in rodents (Best et al., 2005; Wong et al., 2004) and is one of the most potent GSIs (Wolfe, 2009). To test the therapeutic potential of LSN-411575 in NSCLCs, we used mice carrying the above-mentioned Cre-inducible *Kras*^{G12V} oncogenic allele (*Kras*^{LSLG12Vgeo}) together with a tamoxifen-inducible Cre systemically expressed under the RNA polymerase II promoter (Guerra et al., 2003). These mice develop a mixture of lung adenomas (grades 1–3) and adenocarcinomas (grade 4) upon induction with tamoxifen. After

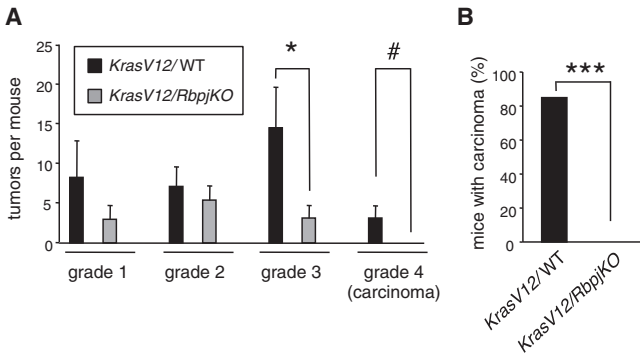

Figure 3. The Canonical Notch Pathway Is Needed for the Generation of *Kras*^{G12V}-Driven NSCLC

(A) Graph depicting the number and grade of tumors per animal. Lungs from *KrasV12*/WT and *KrasV12*/*RbpjKO* mice were pathologically analyzed 5.5–7.5 months after adeno-Cre delivery. For each genotype, n = 7 mice.

(B) Percentage of mice carrying grade 4 (adenocarcinoma) tumors. For each genotype, n = 7 mice.

Values correspond to the average ± SEM. Statistical significance was determined by a two-tailed Student's t test (A) or Fisher's exact test (B): #$p < 0.1$; *$p < 0.05$; ***$p < 0.001$.

See also Figure S2.

6–8 months of the tamoxifen induction, we analyzed changes in tumor size and tumor metabolism by X-ray computed tomography (CT) and positron emission tomography (PET), respectively. Tumors greater than 0.5 mm in diameter were detectable by CT, but only those of grade 4 (i.e. adenocarcinomas) were PET positive (Figures S3A–S3C). Again, this recapitulates the human pathology, in which only malignant tumors are PET positive (Fischer et al., 2001; Gould et al., 2001). Mice carrying *Kras*^{G12V}-driven tumors periodically underwent PET/CT scans, and those carrying at least one PET-positive tumor were randomly allocated into two groups that were treated daily by gavage with vehicle for 15 days or with 3 mg/kg of LSN-411575 for 15 or 22 days.

Previous investigators reported deleterious side effects associated with the use of GSIs, especially in the gut (van Es et al., 2005; Wong et al., 2004). In the case of LSN-411575, it was reported that a dose of 10 mg/kg administered for 15 days in mice produced toxicity in the intestine and weight loss, whereas a dose of 1 mg/kg had no detectable effects and the animals did not lose weight (Wong et al., 2004). In our current study, mice maintained their normal weight after 15 days of treatment with 3 mg/kg, suggesting the absence of deleterious side effects (Figure S3D).

We obtained PET/CT scans of the same mice before and after 15 or 22 days of treatment (Figure 4A). Quantification of the size of the tumors by CT (regardless of whether they were PET positive or negative) revealed that the vehicle-treated tumors increased in size (3.7-fold) after 15 days, whereas the LSN-411575-treated ones grew significantly less than the vehicle-treated controls (1.7-fold after 15 days and 1.2-fold after 22 days; Figure 4B). It is important to note that some of the animals presented atelectasis, which prevents detection by CT. Given the fact that CT cannot discriminate between nonmalignant and malignant tumors, we selectively focused on the response of PET-positive tumors (i.e. adenocarcinomas) and quantified their total ^{18}F-fluor-deoxyglucose (FDG) uptake pre- and post-treatment. In the case of vehicle-treated mice, PET-positive tumors increased their total FDG uptake an average of 2.2-fold during the 15 days of treatment (Figure 4C). In the case of LSN-411575-treated mice, the average change was 0.7-fold after 15 days and 1.0-fold after 22 days (Figure 4C). These results indicate that LSN-411575 has a significant inhibitory effect on the growth of autochthonous murine *Kras*^{G12V}-driven NSCLCs.

Pharmacological Inhibition of γ-Secretase Interferes with ERK Phosphorylation in *Kras*^{G12V}-Driven NSCLCs

Treated *Kras*^{G12V}-driven NSCLCs (see Figure 4C) were analyzed by IHC (samples were obtained 4–8 hr after the last treatment). Our first goal was to evaluate whether the GSI treatment had reached its target, and to that end we used the levels of HES1 as a surrogate marker of γ-secretase activity. In accordance with our previous observations (see Figure 1), the vehicle-treated NSCLCs were strongly positive for HES1 (Figure 5A). In contrast, NSCLCs treated with LSN-411575 for 15 days showed a clear reduction in HES1 levels, confirming that the drug was actually reaching its target within the tumors and at their natural localization (Figure 5A). Also, in agreement with the robust increase in FDG uptake observed during the 15-day interval (Figure 4C), these tumors were highly proliferative (Ki67 staining) and had a low level of apoptosis (activated caspase-3 staining; Figure 5A). NSCLCs treated with LSN-411575 for 15 days presented decreased levels of Ki67-positive cells and a higher frequency of apoptotic cells compared with vehicle-treated tumors (Figure 5A). Of note, these tumors, except for their loss of mitotic cells, retained all other histological features of grade 4 tumors (characteristically defined by the presence of enlarged pleomorphic nuclei exhibiting a high degree of nuclear atypia and multinucleated giant cells) (Jackson et al., 2005). These observations strongly suggest that LSN-411575 arrests cancer growth by inhibiting proliferation and increasing apoptosis.

In an effort to understand the antitumoral effect of LSN-411575, we explored a number of key players in lung cancer, such as ERK (Engelman et al., 2008), AKT (Yang et al., 2008), S6K (Liang et al., 2010), and NFκB (Meylan et al., 2009). In the case of AKT (phospho-Ser473-AKT1), S6K (phospho-Thr389-S6K1), and NFκB (nuclear p65), we could not find any differences between NSCLCs treated for 15 days with vehicle or with LSN-411575 (Figure S4A). However, we did find a remarkable effect on the activity of ERK. In particular, vehicle-treated NSCLCs were strongly positive for pERK1/pERK2 (phospho-Thr202/Tyr204-ERK1 and phospho-Thr185/Tyr187-ERK2), whereas LSN-411575-treated NSCLCs were significantly less positive for pERK (Figure 5A). The results obtained by IHC were confirmed by immunoblotting of tumor extracts. Specifically, we observed lower levels of HES1 and pERK1/pERK2 in LSN-411575-treated (15 days) NSCLCs compared with the corresponding vehicle-treated tumors (Figures 5B and S4B). We wondered whether the lower levels of pERK1/pERK2 were associated with lower levels of its activating kinase, MEK; however, the levels of pMEK1/2 (phospho-Ser217/Ser221-MEK1/2) remained similar in vehicle- and LSN-411575-treated NSCLCs (Figures 5B and S4B), suggesting that the inhibition of pERK

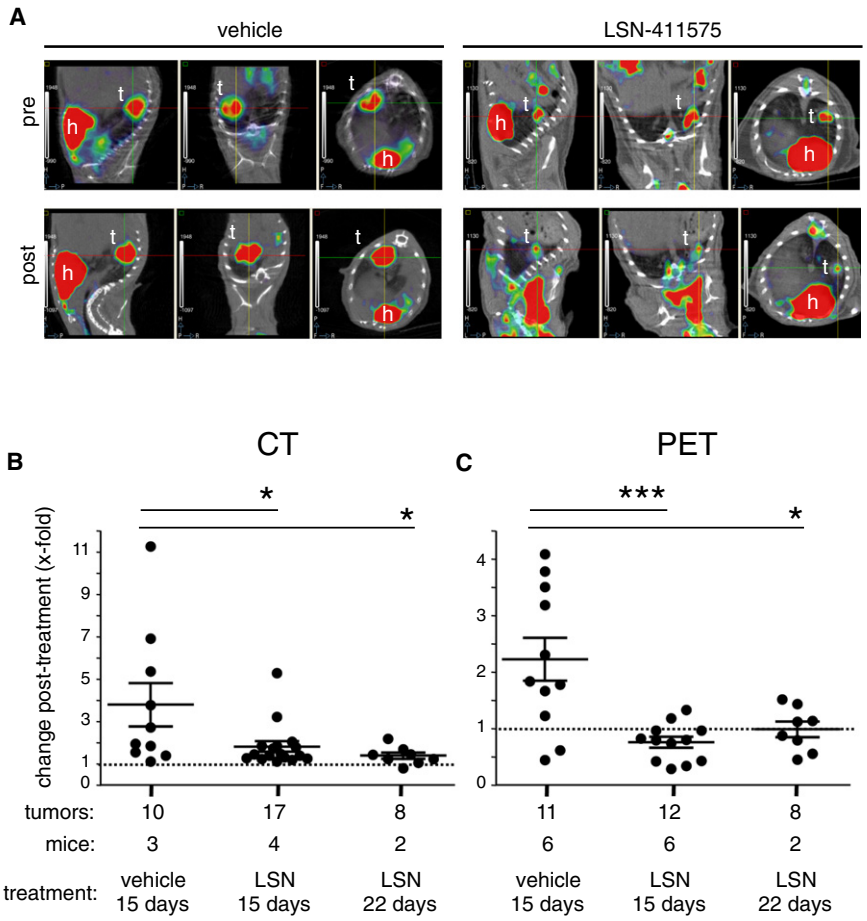

Figure 4. Pharmacological Inhibition of γ-Secretase Arrests *Kras*^{G12V}-Driven NSCLCs

(A) Representative examples of PET/CT analyses of a single *Kras*^{G12V} mouse at the beginning (pre) and end (post) of 15 days of treatment with vehicle (left) or LSN-411575 (right). Images correspond to sagittal (left), coronal (middle), and transverse (right) views. The positions of the PET-positive tumor (t) and the heart (h) are labeled.

(B) Change in total tumor size detected by CT after 15 days of treatment with vehicle, and after 15 or 22 days of treatment with LSN-411575.

(C) Change in total ^{18}F-FDG uptake of PET-positive tumors after 15 days of treatment with vehicle, and after 15 or 22 days of treatment with LSN-411575.

Values correspond to the relative change of each individual tumor from the day before initiation of treatment to the last day of treatment. Bars correspond to the average ± SEM. Top of graph: A two-tailed Student's t test (*$p < 0.05$; ***$p < 0.001$) was used for statistical analysis.

See also Figure S3.

exerted by LSN-411575 is independent of MEK activity. Finally, we wanted to test whether the key observed changes in HES1 and pERK were early events upon initiation of LSN-411575 treatment. We treated mice for 4 days with LSN-411575, and found that the levels of HES1 and pERK in NSCLCs were already lower than in vehicle-treated tumors and similar to those observed in tumors treated with the drug for 15 days (Figure 5C). Collectively, these observations indicate that treatment with LSN-411575 arrests *Kras*^{G12V}-driven NSCLCs in association with inhibition of HES1 expression and ERK phosphorylation.

Inhibition of γ-Secretase Increases DUSP1 in Human and Murine Oncogenic-*Kras* NSCLCs

Previous investigators reported that the Notch pathway upregulates pERK levels in cultured cells in vitro (Kim et al., 2005; Konishi et al., 2007; Michie et al., 2007). However, the mechanisms involved remained unexplored. In an effort to understand the link between the Notch pathway and pERK in the context of lung cancer cells, we focused on the human NSCLC cell line H358, which carries an oncogenic *KRAS* allele (*KRAS*^{G12C}) and requires the activity of the oncogene for its viability (Singh et al., 2009). H358 cells were treated with the GSI DAPT, which is a widely used GSI for assays with in vitro cultured cells (Wolfe, 2009). Recapitulating the results obtained in our lung mouse model, DAPT-treated H358 cells also showed lower levels of pERK (Figure 6A). We also explored two other human *KRAS*-mutated NSCLC cell lines, namely, A549 and H23, which carry *KRAS*^{G12S} and *KRAS*^{G12C} alleles, respectively (Blanco et al., 2009), but whose growth is independent of KRAS activity (Singh et al., 2009). These cell lines also showed decreased levels of pERK upon DAPT treatment (Figure S5A), but the magnitude of the effect was not as pronounced as in KRAS-dependent H358 cells.

To gain insight into the mechanism by which inhibition of the Notch pathway interferes with ERK phosphorylation, we performed RNA microarray analyses to compare GSI-treated and nontreated H358 cells (Table S1). As expected, among the genes that were significantly downregulated by DAPT [false discovery rate (FDR) $p < 0.05$; magnitude $\log_2$ fold change $\leq$ 0.5-fold], we identified *HES1*. Among the genes that showed significant upregulation by DAPT (FDR $p < 0.05$; magnitude $\log_2$ fold change $\geq$ 0.5-fold), we noticed the dual-specificity phosphatases *DUSP1* and *DUSP6*, which are well-known negative regulators of MAP kinases, including ERK (Patterson et al., 2009). Of interest, *DUSP1* is repressed by the Notch pathway in a NSCLC cell line (Haruki et al., 2005); however, we are not aware of a similar link for *DUSP6*. Validation by quantitative RT-PCR (qRT-PCR) confirmed that both the *DUSP1* and *DUSP6* mRNAs were upregulated after treatment of H358 cells with DAPT, whereas *HES1* mRNA levels were downregulated (Figure 6B and Figure S5B). We confirmed that these changes in *HES1* and *DUSP1* mRNA levels correlated with similar changes in the corresponding proteins (Figure 6C). In the case of A549 and H23 cells, both showed a decrease in *HES1* and an upregulation of *DUSP1* upon DAPT treatment; however, only A549 cells presented an upregulation of *DUSP6* (Figures S5B and S5C). In an effort to extrapolate these findings to a different type of Notch-dependent cancer, we performed γ-secretase inhibition of a panel of human T-ALL cell lines. We observed *DUSP1* mRNA

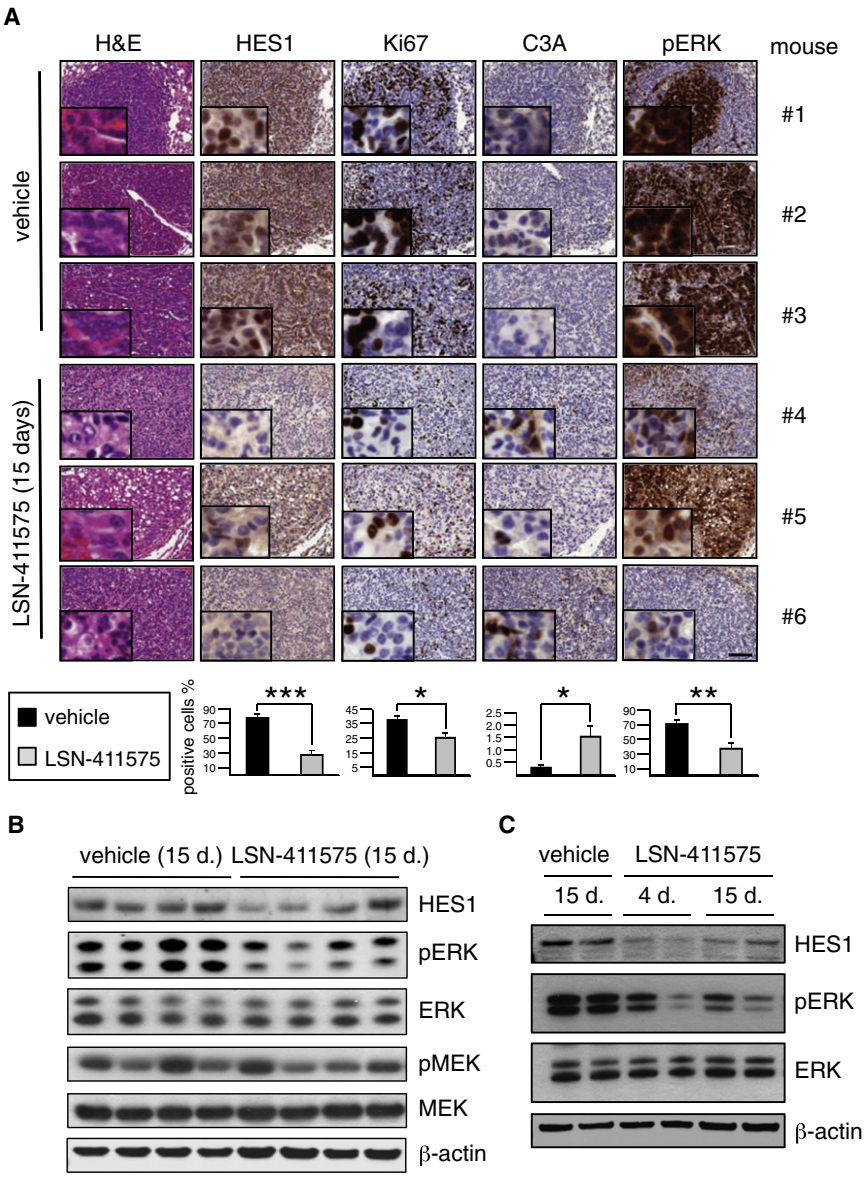

Figure 5. Pharmacological Inhibition of γ-Secretase Diminishes HES1 and pERK in *Kras*^{G12V}-Driven NSCLCs

(A) IHC analyses of NSCLCs after 15 days of treatment with vehicle or LSN-411575. Rows correspond to serial sections of the same tumor. Three examples of vehicle-treated tumors and LSN-411575-treated tumors, each from a different mouse, are shown. All pictures are at the same magnification. The bar in the lower-right panel corresponds to 100 μm. The quantifications shown at the bottom correspond to all of the analyzed NSCLCs: vehicle, 11 tumors (n = 11) present in 6 mice; LSN-411575, 12 tumors (n = 12) present in 6 mice. For each staining, two separate fields at 20× magnification were counted and an average of 1,500 cells were scored per tumor. Values correspond to the average ± SEM. Statistical significance was determined by a two-tailed Student's t test: *p < 0.05; **p < 0.01; ***p < 0.001.

(B) Immunoblotting of the indicated proteins in PET-positive NSCLCs treated for 15 days with vehicle or LSN-411575. Each lane corresponds to a different tumor from a different mouse.

(C) Immunoblotting of the indicated proteins in PET-positive NSCLCs treated with vehicle or LSN-411575 for the indicated periods of time (4 days or 15 days). Each lane corresponds to a different tumor from a different mouse.

See also Figure S4.

upregulation in all of the cell lines, albeit of variable magnitude (Figure S5D), whereas *DUSP6* had an erratic behavior (Figure S5D). These results suggest that the upregulation of *DUSP1* is a general feature of γ-secretase inhibition in cancer.

DUSP1 has been implicated in the dephosphorylation of ERK, JNK, and p38 (Patterson et al., 2009). However, treatment with DAPT resulted in reduced levels of pERK (see Figure 6A) but did not affect the levels of phospho-JNK or phospho-p38 (Figure S5E). We wanted to confirm that DUSP1 was dephosphorylating pERK in our experimental system, and to that end, we ectopically overexpressed a GFP-DUSP1 fusion (Wu et al., 2005) and measured the levels of pERK by immunofluorescence in the GFP-positive cells. Of interest, we observed that H358 cells expressing GFP-DUSP1 had very low levels of pERK upon serum stimulation (10 min), whereas GFP control cells had high levels of pERK under the same conditions (Figures 6D and 6E). Again, we obtained similar results in A549 and H23 cells (Figure S5F). We then performed loss-of-function studies. After testing a total of 12 different interfering RNAs (four siRNAs and eight shRNAs) against *DUSP1*, we observed only a rather modest effect from combining two shRNAs (sh2+sh3; Figure S5G). Despite the partial decrease in DUSP1 levels, expression of the two shRNAs (sh2+sh3) increased the levels of pERK in transfected H358 compared with a scrambled shRNA (shSC; Figure 6F). Moreover, expression of sh2+sh3 abolished the inhibitory effect of DAPT on pERK (Figure 6G), suggesting that the effects of DAPT on pERK are mediated by DUSP1. We also wondered whether DAPT treatment affected the levels of pMEK in H358 cells. We did not observe any changes in pMEK induced by DAPT (Figure S5H), in agreement with our previous observations in GSI-treated tumors (Figures 5B and S4B). These results support the concept that GSI treatment inhibits KRAS signaling through DUSP1 by decreasing the levels of pERK, and without affecting the activity of MEK.

To validate the above data in vivo, we compared the levels of *Dusp1* and *Dusp6* mRNAs in primary murine *Kras*^{G12V}-driven NSCLCs treated for 15 days with LSN-411575 or with vehicle. Of importance, adenocarcinomas from mice treated with LSN-411575 presented increased levels of *Dusp1*/DUSP1 (Figures 6H and 6I) and decreased levels of *Hes1*/HES1 (Figures 5B and 6H) mRNA and protein compared with vehicle-treated adenocarcinomas. In contrast, we did not observe any changes

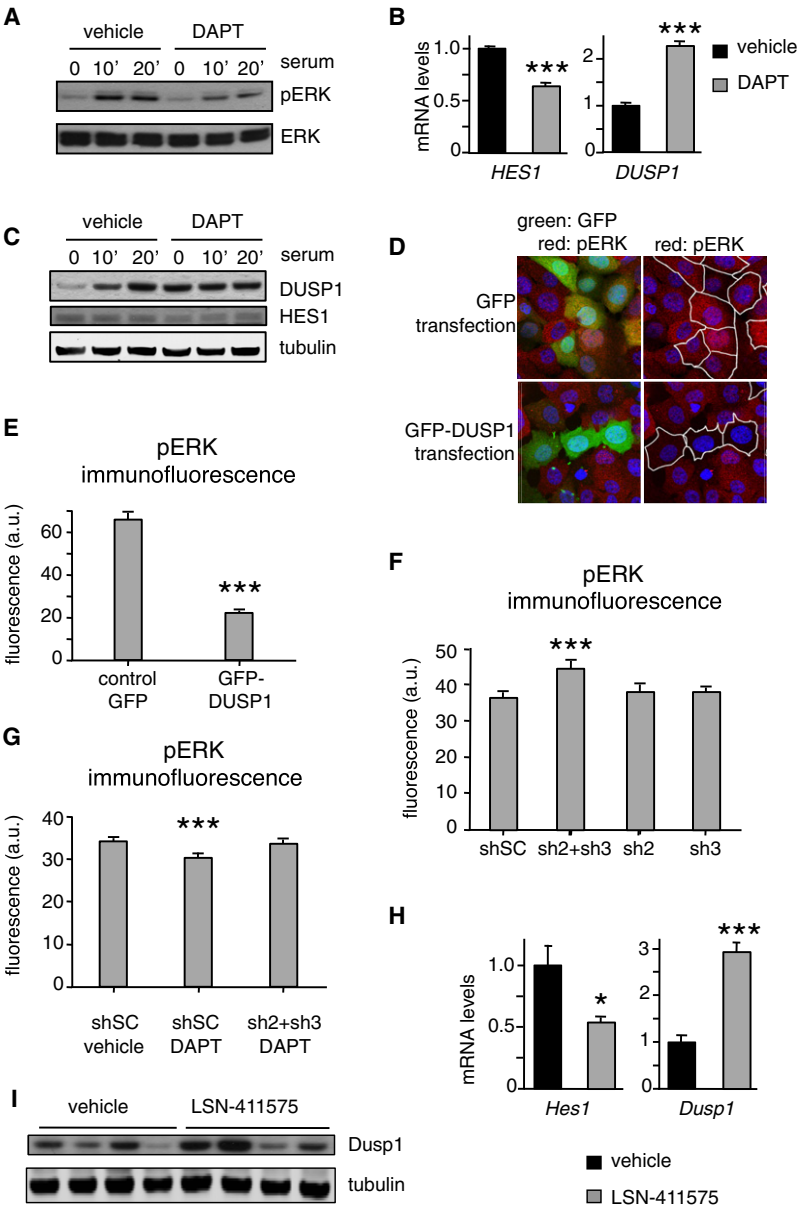

Figure 6. Inhibition of γ-Secretase Increases DUSP1 in Human and Mouse NSCLCs

(A) Analysis of pERK in H358 cells treated with 5 μM DAPT or with vehicle. Cells were treated for 48 hr (36 hr in the presence of serum and then 12 hr in the absence of serum) and then stimulated with serum for the indicated times (in minutes).

(B) Analysis of *DUSP1* and *HES1* expression by qRT-PCR in nontreated (vehicle, n = 3) or DAPT-treated (5 μM DAPT, n = 3) H358 cells. Cells were treated for 48 hr (36 hr in the presence of serum and then 12 hr in the absence of serum).

(C) Analysis of HES1 and DUSP1 in H358 cells treated with 5 μM DAPT or with vehicle. Cells were treated for 48 hr (36 hr in the presence of serum and then 12 hr in the absence of serum) and then stimulated with serum for the indicated times (in minutes).

(D) Fluorescence detection of GFP and phospho-ERK in H358 cells transfected with GFP alone or with a GFP-DUSP1 fusion. Cells were starved and serum stimulated for 10 min. GFP-positive cells are marked with a white line. All images are at the same magnification. The bar in the lower right panel corresponds to 20 μm.

(E) Quantification of the experiment shown in (D). GFP-positive cells (n = 75) were quantified with an automatic software for each transfection (GFP alone, or GFP-DUSP1).

(F) Fluorescence detection of GFP and quantification of phospho-ERK in H358 cells transfected with pGIPZ scramble (shSC), with pGIPZ anti-DUSP1 shRNAs (sh2, sh3, and sh2+sh3). Thirty-six hours after transfection, cells were starved for 12 hr and then serum stimulated for 10 min. GFP-positive cells (n = 120) were quantified with automatic software for each transfection.

(G) Cells were transfected as in (F), and 6 hr after transfection the cells were treated with vehicle or with DAPT (5 μM) for 48 hr (36 hr in the presence of serum and then 12 hr in the absence of serum) and then stimulated with serum for 10 min. GFP-positive cells (n = 120) were quantified with automatic software for each transfection.

(H) Analysis of *Hes1* and *Dusp1* expression by qRT-PCR in PET-positive $Kras^{G12V}$-driven NSCLCs treated with LSN-411575 (n = 4) or vehicle (n = 4) for 15 days.

(I) Immunoblotting of the indicated proteins in PET-positive $Kras^{G12V}$-driven NSCLCs treated for 15 days with vehicle or LSN-411575. Each lane corresponds to a different adenocarcinoma from a different mouse. These adenocarcinomas are the same ones analyzed in Figure 5B and were loaded in the same order.

Values correspond to the average ± SEM. Statistical significance was determined by a two-tailed Student's t test: *$p < 0.05$; ***$p < 0.001$.

See also Figure S5 and Table S1.

in *Dusp6* (Figure S5I). Taken together, these data establish a tight association between HES1 downregulation and DUSP1 induction upon GSI treatment in cancer.

HES1 Directly Binds and Represses the *DUSP1* Promoter

The transcriptional repressor HES1 is a critical mediator of NOTCH1-driven cancer (Wendorff et al., 2010). On the basis of this finding and our above data, we hypothesized that HES1 can repress *DUSP1*. To explore this possibility, we began by performing *DUSP1* promoter assays using a luciferase reporter. Of note, treatment of H358 cells with DAPT induced the *DUSP1* promoter, and this was canceled when HES1 was cotransfected (Figure 7A). These results further reinforce our previous observations that γ-secretase inhibition upregulates the expression of *DUSP1* by downregulating HES1. Additionally, the basal activity of the *DUSP1* promoter was decreased by HES1 expression (Figures 7A and 7B). Also, as a marginal note, treatment of cells with a pharmacological MEK inhibitor (PD0325901) decreased the activity of the *DUSP1* promoter (Figure 7B), in accordance with the known role of MEK as a positive regulator of *DUSP1* expression (Brondello et al., 1997), again suggesting that γ-secretase inhibition exerts its actions in a MEK-independent manner.

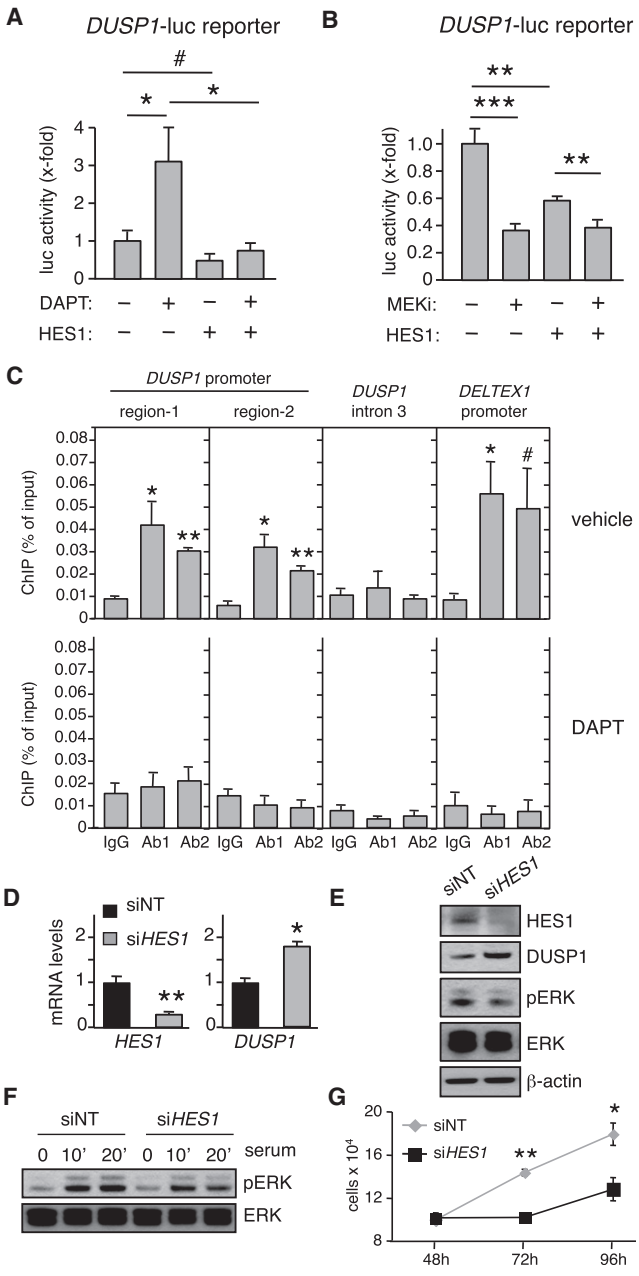

Figure 7. HES1 Directly Binds and Represses the *DUSP1* Promoter

(A) Luciferase activity of H358 cells transfected with a *DUSP1*-luc reporter together with a plasmid expressing HES1 or its corresponding empty control. Cells were treated for 48 hr with 5 μM DAPT or its vehicle in the presence of complete medium.

(B) Luciferase activity of H358 cells transfected with a *DUSP1*-luc reporter together with a plasmid expressing HES1 or its corresponding empty control. Cells were treated for 48 hr with a MEK inhibitor (PD0325901) or its vehicle in the presence of complete medium.

(C) ChIP analysis of the *DUSP1* promoter using two different HES1 antibodies [Ab1, 4H1 (Novus Biologicals) and Ab2, H140 (Santa Cruz Biotechnology)] in H358 cells. Four different DNA regions were analyzed by qPCR: two from the *DUSP1* promoter (see Figure S5), an intronic region from *DUSP1* (intron 3), and the promoter of *DELTEX1*. Cells were treated with 5 μM DAPT or vehicle (ETOH) for 48 hr. Data correspond to three independent biological replicates.

(D) Levels of *HES1* and *DUSP1* expression measured by qRT-PCR in H358 cells treated with si*HES1* (*HES1* siRNA, n = 3) or nontargeting siRNA (siNT, n = 3) for 48 hr (36 hr in the presence of serum and then 12 hr in the absence of serum).

(E) Protein levels of DUSP1, HES1, pERK, and total ERK in H358 cells treated as in (D).

(F) Phosphorylation of ERK in H358 cells treated with si*HES1* (*HES1* siRNA) or siNT for 48 hr (36 hr in the presence of serum and then 12 hr in the absence of serum) and then stimulated with serum for the indicated times (in minutes).

(G) H358 cells were treated with si*HES1* (*HES1* siRNA, n = 3) or siNT (n = 3), and cell numbers were counted at the indicated time points after siRNA transfection.

Values correspond to the average ± SEM. Statistical significance was determined by a two-tailed Student's t test: #$p < 0.1$; *$p < 0.05$; **$p < 0.01$.

See also Figure S6.

Having observed that HES1 has the ability to repress the *DUSP1* promoter, we sought to determine whether HES1 directly binds to the *DUSP1* promoter. HES1 binds two similar sequence motifs, known as class C sites and N-boxes (Iso et al., 2003), and an examination of the human and murine *DUSP1*/*Dusp1* promoters revealed the presence of several putative HES1 binding sites (Figure S6). We tested whether HES1 directly binds to the human *DUSP1* promoter by chromatin immunoprecipitation (ChIP) using two different antibodies against HES1 in H358 cells. Of interest, HES1 immunoprecipitation with two different antibodies resulted in significant enrichment of two regions of the *DUSP1* promoter compared with a control IgG immunoprecipitation (Figure 7C). In contrast, no enrichment was observed when a *DUSP1* intronic region was amplified or when cells were treated with DAPT (Figure 7C). As a positive control, we used the *DELTEX1* promoter, which is directly repressed by HES1 (Zhang et al., 2010). As expected, binding of HES1 to the *DELTEX1* promoter was observed in the absence of DAPT, but not in its presence (Figure 7C).

We wanted to test the effect of *HES1* inhibition on *DUSP1* levels and ERK phosphorylation. Treatment of H358 cells with a pool of siRNAs targeting *HES1* mRNA (si*HES1*) effectively reduced HES1 mRNA and protein levels (Figures 7D and 7E), and, of importance, this resulted in significant upregulation of DUSP1 mRNA and protein levels (Figures 7D and 7E). We previously demonstrated that DUSP1 dephosphorylates pERK (Figures 6D and 6E), and in agreement with this, si*HES1* reduced the levels of phosphorylated ERK (Figures 7E and 7F). Finally, previous reports showed that GSIs can prevent the growth of human cancer cell lines (Chen et al., 2007; Eliasz et al., 2010; Westhoff et al., 2009), and we wondered whether this could also be the case for si*HES1*. Indeed, cells treated with si*HES1* had an impaired proliferative capacity (Figure 7G). All together, these findings show that inhibition of *HES1* in NSCLCs cells recapitulates the effect of DAPT treatment on *DUSP1* expression, ERK phosphorylation, and cell proliferation.

High HES1 and Low DUSP1 Levels Are Associated with Poor Clinical Outcome in Patients with NSCLC

Previous investigators reported that subsets of patients with NSCLC have a hyperactivated Notch pathway (Haruki et al., 2005; Westhoff et al., 2009), which correlates with a poor clinical outcome (Westhoff et al., 2009). In the light of our above results, we wanted to extend this observation to HES1 and examine its relation to DUSP1. We examined the levels of HES1 in a series

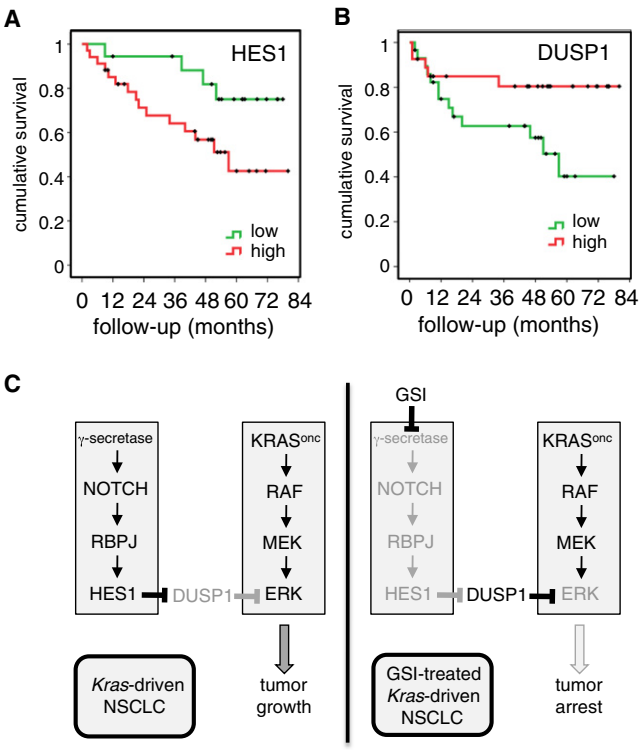

Figure 8. High HES1 and Low DUSP1 Levels Are Associated with Poor Clinical Outcome in Primary Human NSCLCs

(A) Kaplan-Meier curve indicating that patients with NSCLCs with high expression of nuclear HES1 present shorter overall survival ($p = 0.045$). High nuclear HES1 expression corresponds to tumors in which at least 40% of their neoplastic cells are positive for HES1.

(B) Kaplan-Meier curve indicating that patients with NSCLCs with low expression of cytoplasmic DUSP1 present poorer overall survival ($p = 0.048$). Low cytoplasmic DUSP1 expression corresponds to tumors in which <70% of their neoplastic cells are positive for DUSP1.

(C) Summary of the data presented in this work. See Discussion for a detailed explanation.

A logrank test was used to determine statistical significance.

See also Figure S7.

of NSCLCs (n = 82), and observed that tumors with high levels of nuclear HES1 were associated with a shorter overall survival (logrank, $p = 0.045$; Figure 8A and Figure S7A). Previous investigators found a positive correlation between DUSP1 levels and survival in human NSCLCs (Vicent et al., 2004). We confirmed this result in our NSCLC series, in which we obtained a positive correlation between DUSP1 cytoplasmic expression and better overall survival (logrank, $p = 0.048$; Figure 8B and Figure S7A). Moreover, when patients were stratified according to HES1 and DUSP1, those who showed a combination of high HES1 intensity and low DUSP1 expression had the poorest outcome compared with the other three possible combinations (logrank test, $p = 0.09$; Figure S7B). Finally, there was a negative correlation between HES1 intensity and DUSP1 expression (correlation coefficient −0.219; Kendall Tau-b test, $p = 0.07$). Collectively, these observations support the relevance of HES1 in human NSCLCs and reinforce the concept that HES1 represses DUSP1.

DISCUSSION

In this work, we investigated the role of the Notch pathway in the generation and maintenance of primary *Kras*^{G12V}-driven NSCLCs.

Previous studies showed that a significant proportion of patients with NSCLC have a hyperactive Notch pathway (Haruki et al., 2005; Westhoff et al., 2009), but did not examine the role of the Notch pathway in the development of NSCLCs. To address this question, we used a mouse model with a latent *Kras* oncogene that faithfully recapitulates the development of human NSCLCs (Guerra et al., 2003; Jackson et al., 2001; Sweet-Cordero et al., 2005). First, we validated our mouse model by observing that, as in humans, the Notch pathway is hyperactive in murine *Kras*^{G12V}-driven NSCLCs compared with normal lung. This is evidenced by higher levels of active γ-secretase complex, increased levels of NICD (the activated form of NOTCH1), decreased *Numb* mRNA (a negative regulator of the Notch pathway), and increased HES1 protein (a downstream target of the Notch pathway). HES1 protein levels increased in parallel with the degree of malignization, suggesting a requirement of Notch pathway activity during this process. Of note, genetic elimination of either the γ-secretase complex (upstream of the Notch pathway) or *Rbpj* (encoding the canonical DNA-binding partner of NICDs) abolished the formation of *Kras*^{G12V}-driven NSCLCs. These results indicate that the generation of NSCLCs by oncogenic *Kras* requires the activation of the Notch pathway.

On the basis of the above findings, we hypothesized that Notch activity may also be required for the maintenance of primary *Kras*^{G12V}-driven NSCLCs. Previous reports in this direction showed that γ-secretase inhibition slows the growth of subcutaneous xenografts formed by lung cancer cells (Konishi et al., 2007; Luistro et al., 2009; Paris et al., 2005). Xenografts, despite their utility, do not recapitulate the microenvironment of the natural primary tumors, and this may have a critical impact on therapeutic activity, as was elegantly illustrated in the case of pancreatic cancer (Olive et al., 2009). Only a handful of studies have evaluated the efficacy of chemotherapy for primary murine lung tumors (Engelman et al., 2008; Ji et al., 2007; Yang et al., 2008). These studies were largely based on MRI or CT, which cannot discriminate nonmalignant tumors from malignant ones. Here, in an effort to recapitulate a human clinical setting, we also evaluated therapeutic responses by using PET, thus focusing exclusively on malignant tumors. Of importance, mice treated with the pharmacologically active GSI LSN-411575 showed a complete blockade of cancer growth. These results demonstrate that GSIs are therapeutically effective for primary autochthonous *Kras*^{G12V}-driven NSCLCs in mice.

Analyses of LSN-411575-treated, *Kras*^{G12V}-driven NSCLCs indicated a significant reduction in the levels of HES1 as soon as 4 days after treatment, thus confirming that the GSI reached its target. In addition, treated NSCLCs presented decreased proliferation and increased apoptosis. Among a number of key candidate proteins that could be affected by GSI treatment, we selectively detected an effect on the phosphorylation of ERK, which was dramatically reduced after treatment. This observation is in accordance with previous data obtained in in vitro cultured cells, which showed that the Notch pathway upregulates the levels of ERK phosphorylation (Kim et al., 2005; Konishi

et al., 2007; Michie et al., 2007). The role of ERK phosphorylation in *Kras*-driven NSCLCs was recently highlighted by the demonstration that ERK activity is essential for *Kras*-driven lung tumorigenesis (Blasco et al., 2011; Feldser et al., 2010; Junttila et al., 2010). Because MEK is the critical kinase responsible for ERK phosphorylation, we also examined the levels of phosphorylated MEK in GSI-treated NSCLCs; however, in contrast to phospho-ERK, the levels of phospho-MEK were not affected by the GSI. In summary, we found that GSI treatment of primary autochthonous $Kras^{G12V}$-driven NSCLCs impinges on the phosphorylation of ERK without affecting MEK activity.

To dissect the mechanism that links γ-secretase inhibition with dephosphorylation of ERK, we analyzed the transcriptional changes induced by GSI. In particular, we used a human NSCLC cell line, H358, which is addicted to oncogenic *KRAS* (Singh et al., 2009). These cells, as we have shown here, dephosphorylate ERK in response to GSI treatment without affecting phospho-MEK, thus recapitulating the behavior of primary $Kras^{G12V}$-driven NSCLCs. Among the set of genes whose expression was induced by GSI treatment, we focused our attention on the dual-specificity phosphatase DUSP1 because previous data obtained in human NSCLC cells indicate that this phosphatase is regulated by the Notch pathway (Haruki et al., 2005) and dephosphorylates ERK (Lin et al., 2003; Patterson et al., 2009). Indeed, using both gain- and loss-of-function experiments, we confirmed the concept that DUSP1 affects ERK phosphorylation in human H358 cells. Moreover, the induction of *DUSP1* after GSI treatment was confirmed in another two human NSCLC cell lines and in six human T-ALL cell lines, thus giving more general validity to our findings. Finally, we observed *Dusp1* upregulation in GSI-treated murine primary $Kras^{G12V}$-driven NSCLCs. Therefore, the observed association between GSI treatment and *DUSP1* upregulation occurs in the context of primary NSCLCs, and could explain the reduction in ERK phosphorylation upon GSI treatment.

HES1 is a well known transcriptional repressor of multiple genes (Iso et al., 2003; Sang et al., 2010), including genes that are relevant for T-ALL, such as *PTEN* (Palomero et al., 2007) and *CYLD* (Espinosa et al., 2010), which activate AKT and NFκB, respectively. Furthermore, it was recently demonstrated that HES1 plays a critical role in the maintenance of NOTCH1-driven murine T-ALL (Wendorff et al., 2010). Based on our observation that HES1 levels increase in association with malignization and decrease upon GSI treatment of $Kras^{G12V}$-driven NSCLCs, we hypothesized that GSI-induced dephosphorylation of ERK could be mediated by HES1-mediated repression of *DUSP1*. Indeed, luciferase reporter assays supported the concept that HES1 is a negative regulator of *DUSP1*. Furthermore, ChIP showed that HES1 directly binds to and represses *DUSP1*, and that this process can be reverted by GSI treatment. In addition, treatment of H358 cells with si*HES1* promoted a phenotype very similar to that obtained by GSI treatment in terms of ERK phosphorylation, *DUSP1* upregulation, and cell growth arrest.

Finally, we checked the status of HES1 and DUSP1 in primary human NSCLCs. We found that low DUSP1 is associated with poor survival, which is in agreement with previous data (Vicent et al., 2004). In support of our proposed mechanism, we found that high HES1 levels are also associated with poor survival. Moreover, we also observed a suggestive negative correlation between HES1 intensity and DUSP1 expression. These observations support the relevance of HES1 in human NSCLCs and reinforce the concept that HES1 represses DUSP1.

Collectively, our observations establish a direct causal link among γ-secretase inhibition, HES1 downregulation, *DUSP1* derepression, and ERK dephosphorylation (Figure 8C). As mentioned above, high ERK activity is crucial for the development of *Kras*-driven NSCLCs (Blasco et al., 2011; Feldser et al., 2010; Junttila et al., 2010), and, in this regard, we propose that our observation that the Notch pathway is required for NSCLC formation is related to the capacity of HES1 to increase ERK activity through repression of *Dusp1*. Although our current data point to HES1 and DUSP1 as relevant mediators of the effects of GSI treatment on the KRAS signaling pathway, we cannot exclude the possibility that other members of the HES1 family or DUSP1 family, or other unrelated mechanisms, may also participate in mediating the effects of GSI treatment.

The results presented in this work support the therapeutic potential of targeting γ-secretase in NSCLC. We show that GSI treatment inhibits ERK without affecting MEK, and hence we envision a synergistic effect of MEK inhibitors and GSIs on *KRAS*-driven NSCLCs. Of importance, GSIs have been shown to be pharmacologically active in humans (Bateman et al., 2009) and have been tested in clinical trials for Alzheimer disease (Fleisher et al., 2008; Panza et al., 2009; Wolfe, 2009), which could facilitate the evaluation of these compounds for the treatment of human lung cancer, the leading cause of cancer-related deaths in the world.

EXPERIMENTAL PROCEDURES

Mice

Mice were generated by crossing $Kras^{+/LSLG12Vgeo}$ mice (Guerra et al., 2003) with $Psen1^{f/f}$;$Psen2^{-/-}$ (Saura et al., 2004) or $Rbpj^{f/f}$ (Tanigaki et al., 2002) mice. All animal procedures were performed according to protocols approved by the National Cancer Research Center-Instituto de Salud Carlos III (CNIO-ISCIII) Ethics Committee for Research and Animal Welfare.

DNA, RNA, and Protein Analyses

Details regarding the PCR primers, antibodies, and other standard molecular biology methods used in this work are provided in Supplemental Experimental Procedures.

Micro-PET/CT

Imaging was done essentially as described previously (Mulero et al., 2011). See the summary in Supplemental Experimental Procedures.

Treatment with LSN-411575

The LSN-411575 compound was kindly provided by Eli Lilly and Company and formulated in 1% carboxymethyl cellulose, 0.25% Tween 80. The compound was given orally by gavage early in the morning, at a dose of 3 mg/kg/day for the indicated number of days. Control mice were treated with the vehicle following an identical procedure. On the last day of treatment, PET was performed within 2–6 hr after gavage (vehicle- and compound-treated mice were in alternate order for the analysis). Mice were killed within 4–8 hr after gavage, and samples were obtained for pathological and IHC analyses.

Cellular Treatments

H358 human NSCLC cells were purchased from ATCC. Cells were treated with 5 μM DAPT (Calbiochem) for 36 hr in the presence of serum. The cells were then serum starved for 12 hr in the presence of DAPT or vehicle, as indicated in the corresponding figures. When noted, cells were serum stimulated for the

indicated time. For additional details, see Supplemental Experimental Procedures.

Human Samples

Primary lung tumors were collected and handled anonymously at collaborating institutions (Instituto Angel H. Roffo and Hospital Britanico) with the approval of their institutional review boards and following standard ethical and legal protection guidelines regarding human subjects, including informed consent.

Statistical Analysis

Unless otherwise specified, data are presented as mean ± SEM. Student's t test was used to assess the significance of expression levels by both qRT-PCR and IHC. Student's t test was also used to determine the differences among groups for changes in tumor size or animal weight. Associations of protein expression patterns in human TMA of HES1 and DUSP1 were evaluated using the Kendall tau test. Survival curves were tested by logrank test.

ACCESSION NUMBERS

Microarray data were deposited in the National Center for Biotechnology Information's Gene Expression Omnibus (accession number GSE38054).

SUPPLEMENTAL INFORMATION

Supplemental Information includes seven figures, one table, and Supplemental Experimental Procedures and can be found with this article online at http://dx.doi.org/10.1016/j.ccr.2012.06.014.

ACKNOWLEDGMENTS

We thank Mariano Barbacid (CNIO, Madrid, Spain) for kindly providing us with inducible KrasG12V mice and Eli Lilly and Company (Indianapolis, IN) for providing us with LSN-411575. We also thank Andrew Clark (Imperial College London), Anton Bennett (Yale University), Jose F. Rodríguez (National Center of Biotechnology, Madrid, Spain), Ramon Diaz-Uriarte (CNIO), Jose L. de la Pompa (CNIC), and Daniel Muñoz (CNIO) for sharing reagents, giving advice, and critical readings of the manuscript. We also thank all of our clinical collaborators at the Angel H. Roffo and Hospital Britanico (Buenos Aires, Argentina) for their help in obtaining the tumor specimens and for corresponding clinical follow-up. A.M. received a postdoctoral grant from the Miguel Servet Program of the Spanish Ministry of Science. Work in the laboratory of M.S. is funded by the CNIO and by grants from the Spanish Ministry of Science (SAF and CONSOLIDER), the European Research Council (ERC Advanced Grant), and the Marcelino Botin Foundation. A.M. designed and performed most of the experiments and contributed to data analysis, discussion, and writing the manuscript. P.J.F.-M. and D.H. performed some experiments and contributed to data analysis. M.C. performed the murine IHC and pathological analyses. M.M.-M. performed all of the animal manipulations. F.M. performed all analyses of the microPET/CT imaging. D.M. quantified the confocal microscopy. J.S. provided supervision and the mouse model with inducible deletion of γ-secretase. M.S.-Cespedes and M.S.-Carbayo provided the human samples and performed IHC and pathological analyses. T.P. and A.F. gave advice and participated in the design of the study. M.S. designed and supervised the study, secured funding, analyzed the data, and wrote the manuscript. All authors discussed the results and commented on the manuscript.

Received: September 2, 2011
Revised: February 2, 2012
Accepted: June 19, 2012
Published: August 13, 2012

REFERENCES

Bateman, R.J., Siemers, E.R., Mawuenyega, K.G., Wen, G., Browning, K.R., Sigurdson, W.C., Yarasheski, K.E., Friedrich, S.W., Demattos, R.B., May, P.C., et al. (2009). A gamma-secretase inhibitor decreases amyloid-beta production in the central nervous system. Ann. Neurol. *66*, 48–54.

Best, J.D., Jay, M.T., Otu, F., Ma, J., Nadin, A., Ellis, S., Lewis, H.D., Pattison, C., Reilly, M., Harrison, T., et al. (2005). Quantitative measurement of changes in amyloid-beta(40) in the rat brain and cerebrospinal fluid following treatment with the gamma-secretase inhibitor LY-411575 [N2-[(2S)-2-(3,5-difluorophenyl)-2-hydroxyethanoyl]-N1-[(7S)-5-methyl-6-oxo-6,7-dihydro-5H-dibenzo[b,d]azepin-7-yl]-L-alaninamide]. J. Pharmacol. Exp. Ther. *313*, 902–908.

Blanco, R., Iwakawa, R., Tang, M., Kohno, T., Angulo, B., Pio, R., Montuenga, L.M., Minna, J.D., Yokota, J., and Sanchez-Cespedes, M. (2009). A gene-alteration profile of human lung cancer cell lines. Hum. Mutat. *30*, 1199–1206.

Blasco, R.B., Francoz, S., Santamaría, D., Cañamero, M., Dubus, P., Charron, J., Baccarini, M., and Barbacid, M. (2011). c-Raf, but not B-Raf, is essential for development of K-Ras oncogene-driven non-small cell lung carcinoma. Cancer Cell *19*, 652–663.

Brondello, J.M., Brunet, A., Pouysségur, J., and McKenzie, F.R. (1997). The dual specificity mitogen-activated protein kinase phosphatase-1 and -2 are induced by the p42/p44MAPK cascade. J. Biol. Chem. *272*, 1368–1376.

Chen, Y., De Marco, M.A., Graziani, I., Gazdar, A.F., Strack, P.R., Miele, L., and Bocchetta, M. (2007). Oxygen concentration determines the biological effects of NOTCH-1 signaling in adenocarcinoma of the lung. Cancer Res. *67*, 7954–7959.

Chiba, S. (2006). Notch signaling in stem cell systems. Stem Cells *24*, 2437–2447.

Collins, B.J., Kleeberger, W., and Ball, D.W. (2004). Notch in lung development and lung cancer. Semin. Cancer Biol. *14*, 357–364.

Demarest, R.M., Ratti, F., and Capobianco, A.J. (2008). It's T-ALL about Notch. Oncogene *27*, 5082–5091.

Edbauer, D., Winkler, E., Haass, C., and Steiner, H. (2002). Presenilin and nicastrin regulate each other and determine amyloid beta-peptide production via complex formation. Proc. Natl. Acad. Sci. USA *99*, 8666–8671.

Eliasz, S., Liang, S., Chen, Y., De Marco, M.A., Machek, O., Skucha, S., Miele, L., and Bocchetta, M. (2010). Notch-1 stimulates survival of lung adenocarcinoma cells during hypoxia by activating the IGF-1R pathway. Oncogene *29*, 2488–2498.

Engelman, J.A., Chen, L., Tan, X., Crosby, K., Guimaraes, A.R., Upadhyay, R., Maira, M., McNamara, K., Perera, S.A., Song, Y., et al. (2008). Effective use of PI3K and MEK inhibitors to treat mutant Kras G12D and PIK3CA H1047R murine lung cancers. Nat. Med. *14*, 1351–1356.

Espinosa, L., Cathelin, S., D'Altri, T., Trimarchi, T., Statnikov, A., Guiu, J., Rodilla, V., Inglés-Esteve, J., Nomdedeu, J., Bellosillo, B., et al. (2010). The Notch/Hes1 pathway sustains NF-κB activation through CYLD repression in T cell leukemia. Cancer Cell *18*, 268–281.

Feldser, D.M., Kostova, K.K., Winslow, M.M., Taylor, S.E., Cashman, C., Whittaker, C.A., Sanchez-Rivera, F.J., Resnick, R., Bronson, R., Hemann, M.T., and Jacks, T. (2010). Stage-specific sensitivity to p53 restoration during lung cancer progression. Nature *468*, 572–575.

Ferrando, A.A. (2009). The role of NOTCH1 signaling in T-ALL. Hematology (Am Soc Hematol Educ Program) *2009*, 353–361.

Fischer, B.M., Mortensen, J., and Højgaard, L. (2001). Positron emission tomography in the diagnosis and staging of lung cancer: a systematic, quantitative review. Lancet Oncol. *2*, 659–666.

Fleisher, A.S., Raman, R., Siemers, E.R., Becerra, L., Clark, C.M., Dean, R.A., Farlow, M.R., Galvin, J.E., Peskind, E.R., Quinn, J.F., et al. (2008). Phase 2 safety trial targeting amyloid beta production with a gamma-secretase inhibitor in Alzheimer disease. Arch. Neurol. *65*, 1031–1038.

Fraering, P.C. (2007). Structural and functional determinants of gamma-secretase, an intramembrane protease implicated in Alzheimer's disease. Curr. Genomics *8*, 531–549.

Gould, M.K., Maclean, C.C., Kuschner, W.G., Rydzak, C.E., and Owens, D.K. (2001). Accuracy of positron emission tomography for diagnosis of pulmonary nodules and mass lesions: a meta-analysis. JAMA *285*, 914–924.

Guerra, C., Mijimolle, N., Dhawahir, A., Dubus, P., Barradas, M., Serrano, M., Campuzano, V., and Barbacid, M. (2003). Tumor induction by an endogenous

K-ras oncogene is highly dependent on cellular context. Cancer Cell *4*, 111–120.

Haruki, N., Kawaguchi, K.S., Eichenberger, S., Massion, P.P., Olson, S., Gonzalez, A., Carbone, D.P., and Dang, T.P. (2005). Dominant-negative Notch3 receptor inhibits mitogen-activated protein kinase pathway and the growth of human lung cancers. Cancer Res. *65*, 3555–3561.

Hass, M.R., Sato, C., Kopan, R., and Zhao, G. (2009). Presenilin: RIP and beyond. Semin. Cell Dev. Biol. *20*, 201–210.

Heitzler, P. (2010). Biodiversity and noncanonical Notch signaling. Curr. Top. Dev. Biol. *92*, 457–481.

Iso, T., Kedes, L., and Hamamori, Y. (2003). HES and HERP families: multiple effectors of the Notch signaling pathway. J. Cell. Physiol. *194*, 237–255.

Ito, T., Udaka, N., Yazawa, T., Okudela, K., Hayashi, H., Sudo, T., Guillemot, F., Kageyama, R., and Kitamura, H. (2000). Basic helix-loop-helix transcription factors regulate the neuroendocrine differentiation of fetal mouse pulmonary epithelium. Development *127*, 3913–3921.

Jackson, E.L., Willis, N., Mercer, K., Bronson, R.T., Crowley, D., Montoya, R., Jacks, T., and Tuveson, D.A. (2001). Analysis of lung tumor initiation and progression using conditional expression of oncogenic K-ras. Genes Dev. *15*, 3243–3248.

Jackson, E.L., Olive, K.P., Tuveson, D.A., Bronson, R., Crowley, D., Brown, M., and Jacks, T. (2005). The differential effects of mutant p53 alleles on advanced murine lung cancer. Cancer Res. *65*, 10280–10288.

Ji, H., Wang, Z., Perera, S.A., Li, D., Liang, M.C., Zaghlul, S., McNamara, K., Chen, L., Albert, M., Sun, Y., et al. (2007). Mutations in BRAF and KRAS converge on activation of the mitogen-activated protein kinase pathway in lung cancer mouse models. Cancer Res. *67*, 4933–4939.

Junttila, M.R., Karnezis, A.N., Garcia, D., Madriles, F., Kortlever, R.M., Rostker, F., Brown Swigart, L., Pham, D.M., Seo, Y., Evan, G.I., and Martins, C.P. (2010). Selective activation of p53-mediated tumour suppression in high-grade tumours. Nature *468*, 567–571.

Kim, M.Y., Park, J.H., Choi, E.J., and Park, H.S. (2005). Presenilin acts as a positive regulator of basal level activity of ERK through the Raf-MEK1 signaling pathway. Biochem. Biophys. Res. Commun. *332*, 609–613.

Konishi, J., Kawaguchi, K.S., Vo, H., Haruki, N., Gonzalez, A., Carbone, D.P., and Dang, T.P. (2007). Gamma-secretase inhibitor prevents Notch3 activation and reduces proliferation in human lung cancers. Cancer Res. *67*, 8051–8057.

Liang, M.C., Ma, J., Chen, L., Kozlowski, P., Qin, W., Li, D., Goto, J., Shimamura, T., Hayes, D.N., Meyerson, M., et al. (2010). TSC1 loss synergizes with KRAS activation in lung cancer development in the mouse and confers rapamycin sensitivity. Oncogene *29*, 1588–1597.

Lin, Y.W., Chuang, S.M., and Yang, J.L. (2003). ERK1/2 achieves sustained activation by stimulating MAPK phosphatase-1 degradation via the ubiquitin-proteasome pathway. J. Biol. Chem. *278*, 21534–21541.

Luistro, L., He, W., Smith, M., Packman, K., Vilenchik, M., Carvajal, D., Roberts, J., Cai, J., Berkofsky-Fessler, W., Hilton, H., et al. (2009). Preclinical profile of a potent gamma-secretase inhibitor targeting notch signaling with in vivo efficacy and pharmacodynamic properties. Cancer Res. *69*, 7672–7680.

Maraver, A., Tadokoro, C.E., Badura, M.L., Shen, J., Serrano, M., and Lafaille, J.J. (2007). Effect of presenilins in the apoptosis of thymocytes and homeostasis of CD8+ T cells. Blood *110*, 3218–3225.

Meylan, E., Dooley, A.L., Feldser, D.M., Shen, L., Turk, E., Ouyang, C., and Jacks, T. (2009). Requirement for NF-kappaB signalling in a mouse model of lung adenocarcinoma. Nature *462*, 104–107.

Michie, A.M., Chan, A.C., Ciofani, M., Carleton, M., Lefebvre, J.M., He, Y., Allman, D.M., Wiest, D.L., Zúñiga-Pflücker, J.C., and Izon, D.J. (2007). Constitutive Notch signalling promotes CD4 CD8 thymocyte differentiation in the absence of the pre-TCR complex, by mimicking pre-TCR signals. Int. Immunol. *19*, 1421–1430.

Morimoto, M., Liu, Z., Cheng, H.T., Winters, N., Bader, D., and Kopan, R. (2010). Canonical Notch signaling in the developing lung is required for determination of arterial smooth muscle cells and selection of Clara versus ciliated cell fate. J. Cell Sci. *123*, 213–224.

Mulero, F., Donate, L.E., and Serrano, M. (2011). Imaging cancer in mice by PET, CT, and combined PET-CT. Curr Protoc Mouse Biol *1*, 85–103.

Olive, K.P., Jacobetz, M.A., Davidson, C.J., Gopinathan, A., McIntyre, D., Honess, D., Madhu, B., Goldgraben, M.A., Caldwell, M.E., Allard, D., et al. (2009). Inhibition of Hedgehog signaling enhances delivery of chemotherapy in a mouse model of pancreatic cancer. Science *324*, 1457–1461.

Palomero, T., Sulis, M.L., Cortina, M., Real, P.J., Barnes, K., Ciofani, M., Caparros, E., Buteau, J., Brown, K., Perkins, S.L., et al. (2007). Mutational loss of PTEN induces resistance to NOTCH1 inhibition in T-cell leukemia. Nat. Med. *13*, 1203–1210.

Panza, F., Solfrizzi, V., Frisardi, V., Imbimbo, B.P., Capurso, C., D'Introno, A., Colacicco, A.M., Seripa, D., Vendemiale, G., Capurso, A., and Pilotto, A. (2009). Beyond the neurotransmitter-focused approach in treating Alzheimer's disease: drugs targeting beta-amyloid and tau protein. Aging Clin. Exp. Res. *21*, 386–406.

Paris, D., Quadros, A., Patel, N., DelleDonne, A., Humphrey, J., and Mullan, M. (2005). Inhibition of angiogenesis and tumor growth by beta and gamma-secretase inhibitors. Eur. J. Pharmacol. *514*, 1–15.

Patterson, K.I., Brummer, T., O'Brien, P.M., and Daly, R.J. (2009). Dual-specificity phosphatases: critical regulators with diverse cellular targets. Biochem. J. *418*, 475–489.

Roy, M., Pear, W.S., and Aster, J.C. (2007). The multifaceted role of Notch in cancer. Curr. Opin. Genet. Dev. *17*, 52–59.

Sang, L., Roberts, J.M., and Coller, H.A. (2010). Hijacking HES1: how tumors co-opt the anti-differentiation strategies of quiescent cells. Trends Mol. Med. *16*, 17–26.

Saura, C.A., Choi, S.Y., Beglopoulos, V., Malkani, S., Zhang, D., Shankaranarayana Rao, B.S., Chattarji, S., Kelleher, R.J., 3rd, Kandel, E.R., Duff, K., et al. (2004). Loss of presenilin function causes impairments of memory and synaptic plasticity followed by age-dependent neurodegeneration. Neuron *42*, 23–36.

Singh, A., Greninger, P., Rhodes, D., Koopman, L., Violette, S., Bardeesy, N., and Settleman, J. (2009). A gene expression signature associated with "K-Ras addiction" reveals regulators of EMT and tumor cell survival. Cancer Cell *15*, 489–500.

Sweet-Cordero, A., Mukherjee, S., Subramanian, A., You, H., Roix, J.J., Ladd-Acosta, C., Mesirov, J., Golub, T.R., and Jacks, T. (2005). An oncogenic KRAS2 expression signature identified by cross-species gene-expression analysis. Nat. Genet. *37*, 48–55.

Tanigaki, K., Han, H., Yamamoto, N., Tashiro, K., Ikegawa, M., Kuroda, K., Suzuki, A., Nakano, T., and Honjo, T. (2002). Notch-RBP-J signaling is involved in cell fate determination of marginal zone B cells. Nat. Immunol. *3*, 443–450.

Tsao, P.N., Vasconcelos, M., Izvolsky, K.I., Qian, J., Lu, J., and Cardoso, W.V. (2009). Notch signaling controls the balance of ciliated and secretory cell fates in developing airways. Development *136*, 2297–2307.

van Es, J.H., van Gijn, M.E., Riccio, O., van den Born, M., Vooijs, M., Begthel, H., Cozijnsen, M., Robine, S., Winton, D.J., Radtke, F., and Clevers, H. (2005). Notch/gamma-secretase inhibition turns proliferative cells in intestinal crypts and adenomas into goblet cells. Nature *435*, 959–963.

Vicent, S., Garayoa, M., López-Picazo, J.M., Lozano, M.D., Toledo, G., Thunnissen, F.B., Manzano, R.G., and Montuenga, L.M. (2004). Mitogen-activated protein kinase phosphatase-1 is overexpressed in non-small cell lung cancer and is an independent predictor of outcome in patients. Clin. Cancer Res. *10*, 3639–3649.

Weijzen, S., Rizzo, P., Braid, M., Vaishnav, R., Jonkheer, S.M., Zlobin, A., Osborne, B.A., Gottipati, S., Aster, J.C., Hahn, W.C., et al. (2002). Activation of Notch-1 signaling maintains the neoplastic phenotype in human Ras-transformed cells. Nat. Med. *8*, 979–986.

Wendorff, A.A., Koch, U., Wunderlich, F.T., Wirth, S., Dubey, C., Brüning, J.C., MacDonald, H.R., and Radtke, F. (2010). Hes1 is a critical but context-dependent mediator of canonical Notch signaling in lymphocyte development and transformation. Immunity *33*, 671–684.

Westhoff, B., Colaluca, I.N., D'Ario, G., Donzelli, M., Tosoni, D., Volorio, S., Pelosi, G., Spaggiari, L., Mazzarol, G., Viale, G., et al. (2009). Alterations of

the Notch pathway in lung cancer. Proc. Natl. Acad. Sci. USA *106*, 22293–22298.

Wolfe, M.S. (2009). gamma-Secretase in biology and medicine. Semin. Cell Dev. Biol. *20*, 219–224.

Wong, G.T., Manfra, D., Poulet, F.M., Zhang, Q., Josien, H., Bara, T., Engstrom, L., Pinzon-Ortiz, M., Fine, J.S., Lee, H.J., et al. (2004). Chronic treatment with the gamma-secretase inhibitor LY-411,575 inhibits beta-amyloid peptide production and alters lymphopoiesis and intestinal cell differentiation. J. Biol. Chem. *279*, 12876–12882.

Wu, J.J., Zhang, L., and Bennett, A.M. (2005). The noncatalytic amino terminus of mitogen-activated protein kinase phosphatase 1 directs nuclear targeting and serum response element transcriptional regulation. Mol. Cell. Biol. *25*, 4792–4803.

Yang, Y., Iwanaga, K., Raso, M.G., Wislez, M., Hanna, A.E., Wieder, E.D., Molldrem, J.J., Wistuba, I.I., Powis, G., Demayo, F.J., et al. (2008). Phosphatidylinositol 3-kinase mediates bronchioalveolar stem cell expansion in mouse models of oncogenic K-ras-induced lung cancer. PLoS ONE *3*, e2220.

Zhang, P., Yang, Y., Nolo, R., Zweidler-McKay, P.A., and Hughes, D.P. (2010). Regulation of NOTCH signaling by reciprocal inhibition of HES1 and Deltex 1 and its role in osteosarcoma invasiveness. Oncogene *29*, 2916–2926.